CASE STUDY-BASED INSIGHTS ON DISTANCE PROTECTION IN 100% GRID-FORMING INVERTER-DOMINATED TRANSMISSION GRIDS

Moisés J. B. B. Davi[1]* , Vinícius A. Lacerda[2], Andrés Quintero[2], Felipe V. Lopes [3], Oriol Gomis-Bellmunt [2], Mário Oleskovicz[1]

[1]University of São Paulo, Department of Electrical Engineering, São Carlos, Brazil
[2]Universitat Politècnica de Catalunya, Barcelona, Spain
[3]Federal University of Paraíba, Department of Electrical Engineering, João Pessoa, Brazil
**E-mail: moisesdavi@usp.br*

Keywords: DISTANCE PROTECTION, GRID CODE, GRID FORMING, IBR, INVERTER-DOMINATED.

Abstract

As power systems rapidly transition to a landscape dominated by inverter-based resources (IBRs) with grid-forming (GFM) controls, existing protection philosophies face growing challenges. While advancements in GFM technology have primarily focused on system stability, the impact on traditional protection schemes, particularly in the context of evolving grid codes, remains underexplored. In this context, this paper presents a case study-based analysis of how distinct GFM control modes, dictated by grid codes, affect the reliability of conventional distance protection. To do so, a 14-bus, 400 kV network dominated by GFM IBRs was modeled in MATLAB/Simulink, incorporating four fault ride-through (FRT) strategies aligned with recent literature. Several distance protection strategies (self-, cross-, and memory-polarized Mho relays, as well as zero- and negative-sequence polarized quadrilateral characteristics) were assessed. The findings reveal that grid code requirements significantly influence the dependability and security of protection, with virtual-admittance and dual-sequence reactive current injection FRT strategies providing the most consistent performance. In particular, the zero-sequence polarized quadrilateral characteristic exhibited near-perfect dependability for faults involving ground across all evaluated IBR control modes. These results demonstrate the crucial role of harmonized grid code standardization in preserving the reliability of protection systems in modern grids.

1 Introduction

Over the past decades, wind generation has become a vital component of the global power system, propelled by the worldwide energy transition and the increasing penetration of renewable sources [1]. This transformation has led to a rise in the deployment of inverter-based resources (IBRs), with a tendency to now employ grid-forming (GFM) control strategies that are reshaping the operational and protection paradigms of modern grids [2]. While extensive research has addressed aspects of transient and voltage stability [3, 4] in systems with GFM IBRs, the fundamental question of how conventional protections are affected in such GFM IBR-dominated systems remains underexplored. Most research in this topic focuses on grid-following (GFL) IBRs operating in systems where conventional generators prevail [5–8].

The report presented in [2] highlights this research gap by identifying only two studies that directly address the protection of systems with GFM IBRs [9, 10]. In [9], three converter architectures were examined in consideration of fault-ride-through (FRT) requirements through current control and virtual impedance methods. The study demonstrated that, depending on the adopted design, the adverse influence of GFM IBRs on distance protection performance can be reduced. However, the analyses were restricted to phase-to-phase (PP) faults with a fixed fault resistance of 1 Ω, and 100% IBR-dominated grids were not explored. Similarly, [10] extended the investigation by assessing distance protection performance with quadrilateral characteristics and a phase-selection algorithm based on incremental currents. Two GFM IBR structures were tested (one employing a GFM/GFL operational transition during faults and another based on virtual impedance), and the results indicated that virtual-impedance-based control provides superior dependability, yet two-phase-to-ground (PPG) faults were omitted, fault resistance was fixed at 2 Ω, and 100% IBR-dominated systems were again not addressed.

Further progress was achieved in [11, 12], which expanded the understanding of distance protection behavior in systems containing GFM inverters. In [11], the performance of quadrilateral ground and Mho phase protections was analyzed under single- and two-phase faults with fault resistances up to 20 Ω, assessing dependability and security aspects. Building upon that, [12] extended the fault resistance to 50 Ω and conducted an impedance-trajectory and phase-comparator analysis. Both studies consistently demonstrated the detrimental effect of increasing fault resistance on distance protection performance, although three-phase faults were not included. Another contribution came from [13], which evaluated multiple conventional protection functions for 100% IBR-dominated grids, including a negative-sequence impedance-based directional protection, a

current-angle-based phase-selection method, and four polarization approaches for Mho-type distance protection (self-, cross-, memory-, and memory-cross-polarized). Simulations compared conventional and inverter-dominated systems under distinct GFM control modes, highlighting the importance of harmonized grid codes to ensure consistent protection behavior. Nevertheless, that work did not consider quadrilateral distance characteristics for phase-to-ground (PG) faults, nor did it examine virtual-admittance-based controls [14].

In general, the existing studies are complementary and offer significant progress in the protection scope for 100% IBR-dominated systems, but do not provide an integrated perspective that simultaneously considers multiple grid code requirements for IBRs, the key distance protection characteristics and polarization strategies, and a broad scope of faults concerning their types and the resistances.

In this context, the present study performs electromagnetic-transient (EMT) simulations to investigate the interplay between GFM IBR control requirements, aligned with recent literature, and conventional distance protection strategies. A test system representing a fully inverter-dominated network was modeled in MATLAB/Simulink to replicate realistic fault conditions. The analysis focuses on five protection strategies commonly used in practice: self-, cross-, and memory-polarized Mho relays, as well as zero- and negative-sequence polarized quadrilateral characteristics [15]. Four FRT strategies are assessed to represent different grid code strategies prioritizing positive-sequence active current [16], positive-sequence reactive current [17], both positive- and negative-sequence reactive currents [18], or maintaining the virtual-admittance control approach controlling the reference currents during faults [14].

The main idea is to provide a case study in which, for the same 100% GFM IBR-dominated system, the influence of different FRT strategies on the performance of distinct distance protection strategies is assessed, showing how certain grid codes may favor or hinder specific distance protection behaviors. The resulting findings are expected to shed light on the protection challenges of future inverter-based grids and contribute to ongoing efforts to standardize and coordinate protection in next-generation power systems.

2 Test System

To assess the performance of various protection schemes under the described conditions, a detailed EMT model of a GFM IBR-dominated transmission network was developed in MATLAB/Simulink software. The modeled system consists of 14 buses operating at 400 kV (50 Hz) [19], incorporating 11 GFM IBRs and 9 loads distributed throughout the network. The individual line lengths are specified in Fig. 1 as well as IBR and load power ratings.

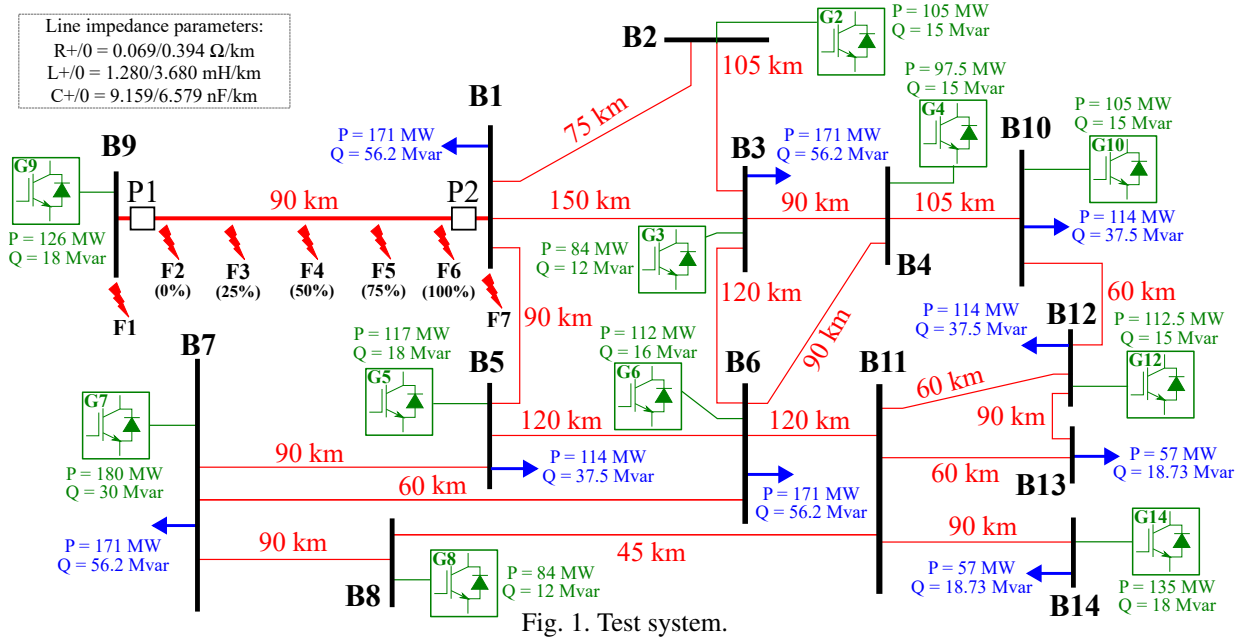

Fig. 1. Test system.

Table 1 GFM IBR main parameters.

Parameter	G2,G3,G4,G12	G5,G10,G14	G6,G7,G8	G9
Nominal Power (MVA)	150,120,150,150	180,150,180	160,300,120	180
Virtual Inertia (s)	2.5	1	2	2
Virtual Damping	180	100	150	120
Virtual Reactance (p.u.)	0.5	0.5	0.5	0.5
Virtual Admitt. Time Constant (s)	15e-3	15e-3	15e-3	15e-3
Filter Reactance (p.u.)	0.1	0.1	0.1	0.1
Filter Resistance (p.u.)	5e-4	5e-4	5e-4	5e-4

Regarding the modeling of the GFM inverters, the main parameters are described in Table 1. The virtual admittance control concept was adopted, as described in [14]. The Double Synchronous Reference Frame (DSRF) approach was employed within the GFM control structure, enabling independent regulation of both positive- and negative-sequence voltages and currents. For synchronization, the Virtual Synchronous Machine (VSM) control principle was implemented [20, 21]. The positive-sequence voltage reference is determined through a Q/Vac droop control, while the negative-sequence voltage reference is fixed at zero. These two sequence components are superimposed to generate the final three-phase (abc) voltage reference supplied to the converter.

The converter transitions to an abnormal operating mode when the positive-sequence voltage magnitude drops below 0.85 p.u., or when the negative-sequence voltage exceeds 0.05 p.u. Under such abnormal conditions, negative-sequence current injection is prioritized [22]. The K-factor for positive- and negative-sequence reactive curves was set to 2.5 [18].

During abnormal operation, four different FRT strategies were analyzed. These alternative control modes are summarized as follows:

- **C1**: priority to positive-sequence active current, as commonly prescribed in early grid codes [16];
- **C2**: priority to positive-sequence reactive current, in line with more recent FRT requirements that favor voltage support during faults [17];
- **C3**: priority to both positive- and negative-sequence reactive currents, following modern grid codes that explicitly require negative-sequence current injection for asymmetrical faults [18];
- **C4**: virtual-admittance-based control, in which the converter currents are fully defined by the virtual admittance law even during faults, without enabling a dedicated FRT current-prioritization logic. In this mode, the virtual-admittance current references are only limited in magnitude to 1 p.u., with no predefined priority between active and reactive components [14].

For the fault analysis performed in this study, disturbances were applied to the transmission line connecting buses B1 and B9. Both internal faults F2 to F6, corresponding respectively to 0%, 25%, 50%, 75%, and 100% of the line length, and external faults (F1 and F7, corresponding to bus B9 and bus B1 faults, respectively) were considered. The fault scenarios included multiple fault types (AG, AB, ABG, and ABC), resistances (varying the phase-to-phase resistance between 0, 1.5, 2.5, and 5 Ω, and the phase-to-ground resistance between 0, 10, 25, and 50 Ω), and inception angles (0 and 90 degrees). For all presented analyses, measurements taken at point P1 were used as the reference for evaluation.

3 Assessed Distance Protections

This section discusses the distance protection strategies considered in this study, including the Mho and Quadrilateral characteristics [15].

The behavior of the assessed distance protections is governed by the evaluation of the operating ($\overrightarrow{V_{op}}$) and polarizing ($\overrightarrow{V_{pol}}$) quantities, which are described for the AG and AB fault loops in Table 2 for Mho characteristics [15]. Formulations for other faulted loops can be obtained analogously by replacing the respective phase variables [15]. In Table 2, Z_R denotes the impedance setting of the protection zone; $\overrightarrow{I_A}$, $\overrightarrow{I_B}$, and $\overrightarrow{I_0}$ are the phase-A, phase-B, and zero-sequence current phasors, respectively; while $\overrightarrow{V_A}$, $\overrightarrow{V_B}$, and $\overrightarrow{V_C}$ correspond to the phase voltage phasors. The coefficient k_0 represents the zero-sequence compensation factor, and the subscript $_M$ designates memorized (pre-fault) quantities [23].

In this study, the phase-comparison principle is adopted. The comparator angle, α, is obtained as the phase difference between the operating and polarizing quantities. The distance element identifies a fault as internal to its zone of protection whenever α lies within the interval $\pm 90^\circ$.

Regarding the quadrilateral characteristics, four phase comparators are evaluated: the reactance element, the directional element, the left blinder, and the right blinder. Quadrilateral characteristics with negative- (Quadr. I_2) and zero-sequence (Quadr. I_0) current as polarization were considered. The quantities for each element are described in Table 3.

In this table, $\overrightarrow{V_{loop}}$ and $\overrightarrow{I_{loop}}$ represent the loop voltage and current phasors; $\overrightarrow{I_2}$ is the negative-sequence current phasor; ϕ represents the non-homogeneity angle; Z_D is the impedance of

Table 2 Operating and Polarizing Quantities for Mho Characteristics (AG and AB Fault Loops).

Mho Self-Polarized Distance Protection (Mho Self)		
Loop	$\overrightarrow{V_{op}}$	$\overrightarrow{V_{pol}}$
AG	$Z_R \cdot (\overrightarrow{I_A} + k_0 \cdot \overrightarrow{I_0}) - \overrightarrow{V_A}$	$\overrightarrow{V_A}$
AB	$Z_R \cdot (\overrightarrow{I_A} - \overrightarrow{I_B}) - (\overrightarrow{V_A} - \overrightarrow{V_B})$	$(\overrightarrow{V_A} - \overrightarrow{V_B})$
Mho Memory-Polarized Distance Protection (Mho Mem)		
Loop	$\overrightarrow{V_{op}}$	$\overrightarrow{V_{pol}}$
AG	$Z_R \cdot (\overrightarrow{I_A} + k_0 \cdot \overrightarrow{I_0}) - \overrightarrow{V_A}$	$\overrightarrow{V_{A_M}}$
AB	$Z_R \cdot (\overrightarrow{I_A} - \overrightarrow{I_B}) - (\overrightarrow{V_A} - \overrightarrow{V_B})$	$(\overrightarrow{V_A} - \overrightarrow{V_B})_M$
Mho Cross-Polarized Distance Protection (Mho Cross)		
Loop	$\overrightarrow{V_{op}}$	$\overrightarrow{V_{pol}}$
AG	$Z_R \cdot (\overrightarrow{I_A} + k_0 \cdot \overrightarrow{I_0}) - \overrightarrow{V_A}$	$j(\overrightarrow{V_B} - \overrightarrow{V_C})$
AB	$Z_R \cdot (\overrightarrow{I_A} - \overrightarrow{I_B}) - (\overrightarrow{V_A} - \overrightarrow{V_B})$	$-j\overrightarrow{V_C}$

Table 3 Operating and Polarizing Quantities for Quadrilateral Characteristics.

Element	$\overrightarrow{V_{op}}$	$\overrightarrow{V_{pol}}$
Reactance	$Z_R \cdot \overrightarrow{I_{loop}} - \overrightarrow{V_{loop}}$	$(j\overrightarrow{I_0} \mid j\overrightarrow{I_2}) \cdot e^{j\phi}$
Directional	$Z_D \cdot (\overrightarrow{I_0} \mid \overrightarrow{I_2})$	$\overrightarrow{V_{loop\,M}}$
Right blinder	$Z_{Rb} \cdot \overrightarrow{I_{loop}} - \overrightarrow{V_{loop}}$	$Z_{Rb} \cdot \overrightarrow{I_{loop}}$
Left blinder	$Z_{Lb} \cdot \overrightarrow{I_{loop}} - \overrightarrow{V_{loop}}$	$Z_{Lb} \cdot \overrightarrow{I_{loop}}$

the directional characteristic (unit magnitude and phase angle equal to that of Z_R); and Z_{Rb} and Z_{Lb} correspond to the right and left blinders, respectively [24].

The settings for Z_R, Z_D, Z_{Lb}, and ϕ are 31.2∠80.3°, 1∠80.3°, 5 Ω, and 8°. Z_{Rb} was configured as 4·$|Z_R|$Ω for PG and PPG faults, and $|Z_R|$Ω for PP and PPP faults [24].

4 Results and Discussions

This section presents and discusses the main insights obtained in this study, providing a quantitative overview of the dependability (the ability of a protection to operate when expected, i.e., in the occurrence of internal faults) and security (its ability to prevent unnecessary trips under external fault conditions) for each protection function, by fault type and IBR control mode considered.

4.1 Overall Dependability and Security Results of the Evaluated Protections

This subsection presents analyses focusing primarily on dependability and security, with numerical results summarized in Table 4. Among the main observations derived from this preliminary analysis, the following stand out:

- **Mho Self:** Although it achieved 100% security regardless of the fault type or IBR control mode, it was also the only evaluated function that showed unsatisfactory dependability levels for all assessed conditions, with percentages below or equal to 50%. Thus, this strategy should be avoided in systems such as the one analyzed in this paper;
- **Mho Mem:** This protection was the best-performing for PP faults when operating under control C4, with dependability and security values above 96%. This behavior suggests that the virtual admittance control strategy best aligns IBR behavior with that of conventional synchronous generators, for which memorized Mho characteristics were originally designed. Moreover, this protection achieved 100% dependability for PG, PP, and PPG faults under C2 and C3 controls, although with lower security levels (indicating zone overreach). Additionally, it was the best-performing for PPP faults, delivering 100% security (except for C1) and dependable performance above 62% across all IBR control modes;
- **Mho Cross:** The cross-polarized strategy proved to be highly effective for PP faults under control mode C3, achieving 100% dependability and security, confirming conclusions already observed in the literature [13]. Satisfactory performance was also recorded for PP faults under control C4, though not exceeding the outcomes achieved with the Mho Mem;
- **Quadr. $\overrightarrow{I_0}$:** This protection yielded 100% dependability and security for PG faults in all cases except control C1, which still presented results above 93%. As PG faults are the most frequent in transmission systems, these findings are particularly relevant for protection design in IBR-dominated networks. It also performed excellently for PPG faults under more recent control modes (C3 and C4), maintaining 100% security and dependability above 85%. Notably, under control C3, this protection reached 100% dependability and security for both PG and PPG faults;
- **Quadr. $\overrightarrow{I_2}$:** As expected, this protection displayed non-zero dependability only for controls C3 and C4, which allow IBRs to inject negative-sequence current ($\overrightarrow{I_2}$) during asymmetrical faults. However, its performance was not the best for any specific fault type or control mode combination.

Overall, the results highlight the high potential of the Quadr. $\overrightarrow{I_0}$ protection for PG faults across all control modes, with particularly promising outcomes under C2, C3, and C4. This strategy also performed well for PPG faults, especially for modern control configurations (C3 and C4). For PP faults, none of the evaluated protections achieved satisfactory results across all control modes simultaneously, although the Mho Cross stood out under C3, and the Mho Mem under C4. Finally, for PPP faults, the Mho Mem was the most consistent, maintaining 100% security and more than 62% dependability across C2, C3, and C4 controls.

Table 4 Dependability and security percentages of the evaluated protection functions.

Dependability / Security (%)				
Mho Self				
Fault Type	C1	C2	C3	C4
PG	21.1/100	21.9/100	21.9/100	23.4/100
PP	31.3/100	31.3/100	31.3/100	37.5/100
PPG	30.5/100	31.3/100	36.7/100	34.4/100
PPP	50.0/100	40.6/100	34.4/100	43.8/100
Mho Mem				
Fault Type	C1	C2	C3	C4
PG	47.7/59.4.3	100/20.8	100/29.2	98.4/56.3
PP	6.35/33.3	100/50.0	100/33.3	96.9/100
PPG	4.69/20.8	100/68.7	100/75.0	86.7/95.8
PPP	93.8/0.00	71.9/100	65.6/100	62.5/100
Mho Cross				
Fault Type	C1	C2	C3	C4
PG	18.0/100	18.0/100	53.9/87.5	46.9/100
PP	0.00/100	6.25/100	100/100	75.0/100
PPG	25.0/100	32.8/100	100/66.7	75.0/100
PPP	50.0/100	40.6/100	50.0/100	43.8/100
Quadr. $\overrightarrow{I_0}$				
Fault Type	C1	C2	C3	C4
PG	96.9/93.8	100/100	100/100	100/100
PPG	78.1/100	49.2/91.7	100/100	85.9/100
Quadr. $\overrightarrow{I_2}$				
Fault Type	C1	C2	C3	C4
PG	0.0/93.8	0.0/100	87.5/100	80.5/100
PP	0.0/75.0	0.0/100	93.8/66.7	75.0/83.3
PPG	0.0/100	0.0/100	96.1/47.9	76.6/45.8

4.2 Detailed Discussions by Fault Type

Figs. 2, 3, 4, and 5 illustrate the correct operation rate of distance protections for PG, PP, PPG, and PPP faults, respectively, considering each fault location (F1 to F7) and each IBR control mode under analysis. These figures represent the percentage of cases in which the protection did not operate for external faults (F1, F6, and F7) and operated for internal faults (F2 to F5).

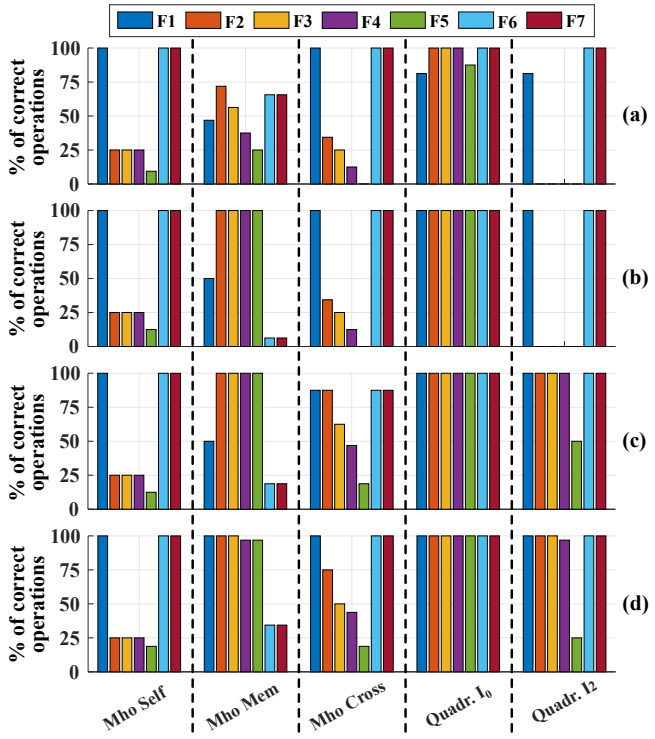

Fig. 2 Performance of distance protections for PG faults, considering the IBR controls: (a) C1, (b) C2, (c) C3, and (d) C4.

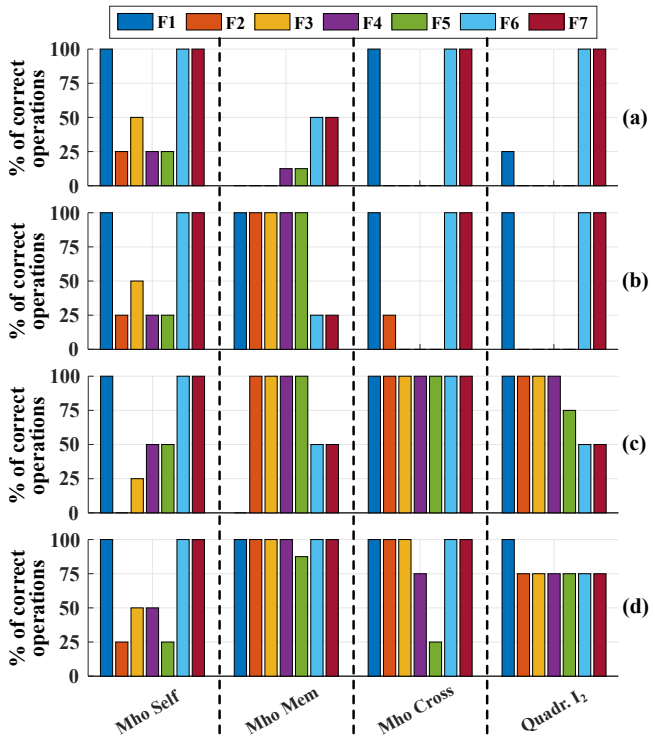

Fig. 3 Performance of distance protections for PP faults, considering the IBR controls: (a) C1, (b) C2, (c) C3, and (d) C4.

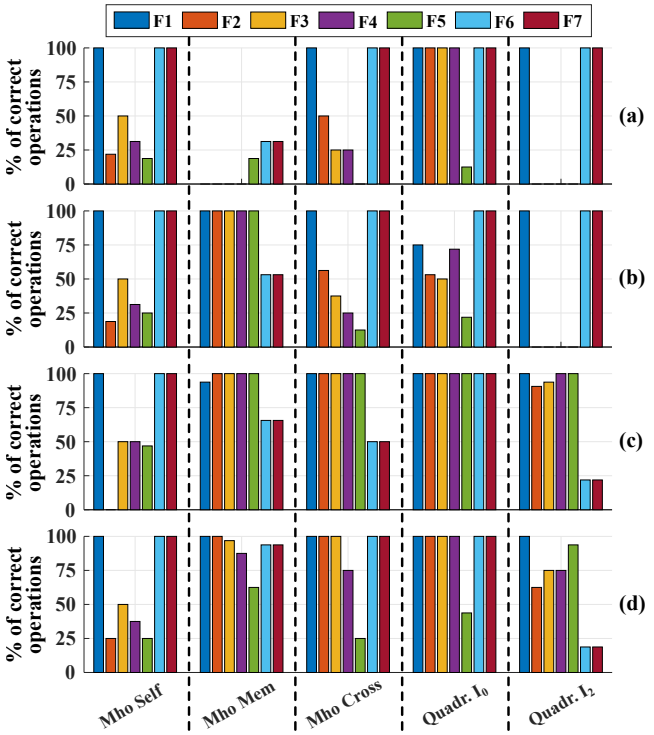

Fig. 4 Performance of distance protections for PPG faults, considering the IBR controls: (a) C1, (b) C2, (c) C3, and (d) C4.

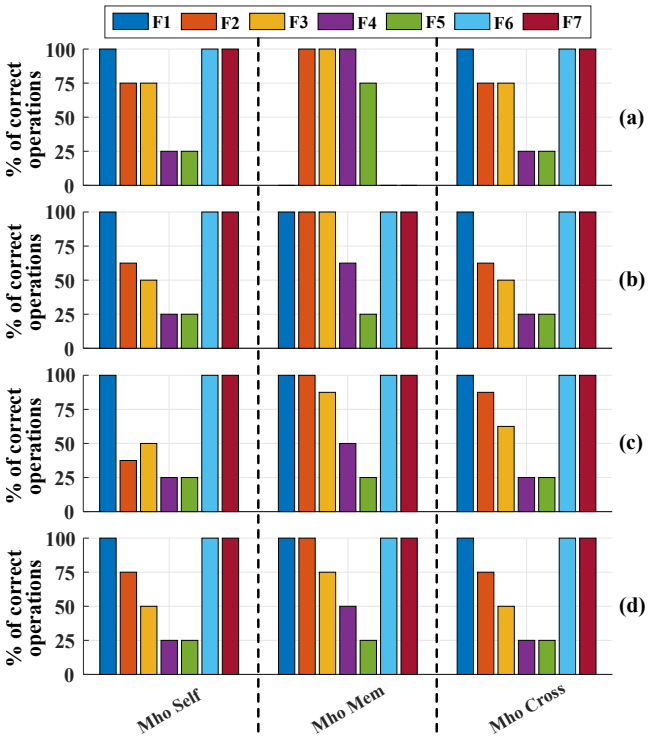

Fig. 5 Performance of distance protections for PPP faults, considering the IBR controls: (a) C1, (b) C2, (c) C3, and (d) C4.

Fig. 2 shows a consistent improvement trend in the accuracy of distance protections for PG faults as the control modes evolve from C1 to C4, particularly for the Mho Mem, Mho Cross, and Quadr. $\overrightarrow{I_2}$. The Quadr. $\overrightarrow{I_0}$ exhibits a uniform behavior across all internal fault locations from C2 onward, combining 100% satisfactory performance for internal faults with complete stability for external ones, which confirms its strong suitability for ground faults already suggested by the aggregated results. In contrast, the Mho Self characteristic presents a marked underreach pattern: its operation is concentrated in the most severe internal faults close to the measurement point (P1), with low sensitivity to faults closer to the remote terminal. This explains the low dependability levels observed in Table 4, despite the consistently high security.

The performance improvement observed from C3 to C4 is strongly linked to the changes in IBR fault-current behavior. Under C3, IBRs start injecting negative-sequence currents during asymmetrical faults, making the system response more similar to that of synchronous generators. The virtual-admittance control (C4) further stabilizes the apparent impedance seen by the relay, consolidating these gains in terms of correct-operation rate.

Fig. 3 indicates that, for PP faults, all protections show limited performance under C1 and C2. Under control C3, a significant improvement is observed, especially for the Mho Cross function, which achieves 100% accuracy across all scenarios. This behavior suggests that the application of cross-polarization facilitates maintaining correct directional discrimination, even under the angular variation characteristics imposed by IBRs with C3-type controls [13]. The use of control C4 consolidates these improvements, particularly for the Mho Mem, which achieves accuracy levels above 90% under all conditions. The Quadr. $\overrightarrow{I_2}$, which strongly depends on the negative-sequence component, also demonstrates satisfactory performance under C3 and C4, though still inferior to the Mho-based strategies, reflecting its higher sensitivity to the dynamic characteristics of GFM-IBR control schemes.

For PPG faults (Fig. 4), the transition from C1 to the more advanced control modes again leads to a substantial improvement in protection performance. The Mho Self continues to display low performance for internal faults (showing an underreach tendency), whereas the other protection strategies exhibit significantly higher accuracy levels under C3 and C4 controls. The Quadr. $\overrightarrow{I_0}$ is the function that most closely approaches ideal behavior for PPG faults, especially under C3, with full coverage of internal faults and stable performance for external ones. Mho Mem and Mho Cross provide intermediate yet robust performance, confirming that adequate polarization and advanced IBR controls are key to ensuring dependable distance protection under complex unbalanced fault conditions.

Finally, Fig. 5 shows that for PPP faults, except for the Mho Mem under control C1, all distance protections display an underreach pattern for resistive internal faults, which becomes more pronounced as the fault point moves further away from the measurement point P1. From C2 to C4, all evaluated functions remain fully secure for external faults, indicating that the main challenge in PPP scenarios is achieving sufficient reach rather than avoiding false tripping. Among the tested schemes, Mho Mem attains the highest correct-operation rates, followed by Mho Cross, whereas Mho Self maintains the lowest sensitivity to internal PPP faults.

5 Conclusions

This case study provided insights about distance protection behavior in 100% GFM IBR-dominated systems, emphasizing the influence of grid code FRT requirements on protection reliability. The main contributions and remarks can be summarized as follows:

- The evolution from active-current priority (C1) to dual-sequence-reactive current priority (C3) and virtual-admittance (C4) control modes substantially increased the dependability of the assessed protection functions, proving that FRT prescriptions directly shape the apparent impedance and angular relationships perceived by distance relays;
- Among all evaluated functions, the Quadr. $\overrightarrow{I_0}$ consistently achieved the highest dependability and security in PG and PPG faults, confirming its suitability for modern IBR grids;
- The Mho Mem and Mho Cross performed robustly under advanced controls (C3 and C4), especially for PP and PPP faults, reflecting the stabilizing effect of voltage memory and cross-polarization in preserving directional integrity;
- The Mho Self, although fully secure (no false tripping), demonstrated insufficient dependability in all tested scenarios, reinforcing its unsuitability for GFM IBR-dominated networks.

Overall, this study highlights the interplay between GFM converter behavior, grid code standardization, and distance protection philosophy, offering insight into how future regulatory evolution can secure dependable fault detection in increasingly inverter-dominated power systems.

Beyond the specific FRT control modes investigated in this paper, it is important to recognize that additional internal variations of GFM IBR controllers, such as current saturation and prioritization strategies, can also affect fault current behavior and, in turn, the response of protection schemes. Such implementation-dependent aspects were not exhaustively explored in this work and therefore deserve dedicated attention in future studies. In addition, future work will extend this analysis to analytical modeling of distance protection under GFM dynamics, including simplified fault-current and voltage phasor formulations to explain the observed results and to support the development of novel protection solutions for IBR-dominated grids.

6 Acknowledgements

This work was supported by the São Paulo Research Foundation (FAPESP) (grant #2024/17884-3), as well as by the Coordination for the Improvement of Higher Education Personnel (CAPES) and the National Council for Scientific and Technological Development (CNPq #309184/2023-1 and

#306441/2025-0). Additionally, it has been supported by the MCIN/AEI HP2C-DT project (grant TED2021-130351B-C21) and co-funded by the European Union NextGenerationEU/PRTR. The work of Oriol Gomis-Bellmunt was supported by the Institució Catalana de Recerca i Estudis Avançats (ICREA). We gratefully acknowledge the support of the RCGI – Research Centre for Greenhouse Gas Innovation, hosted by the University of São Paulo (USP), sponsored by FAPESP [#2020/15230-5], and sponsored by TotalEnergies and the strategic importance of the support given by ANP (Brazil's National Oil, Natural Gas and Biofuels Agency) through the R&DI levy regulation.

References

[1] J. Lee and F. Zhao. (2025) Global wind report 2025.

[2] U. Münz *et al.*, "Protection of 100% inverter-dominated power systems with grid-forming inverters and protection relays - gap analysis and expert interviews," *SANDIA REPORT - SAND2024-04848*, 04 2024.

[3] C. Collados Rodriguez *et al.*, "Grid-following and grid-forming converter control comparison under fault conditions," in *12th Energy Conversion Congress & Exposition*, 2021, pp. 598–603.

[4] D. Pan, X. Wang, F. Liu, and R. Shi, "Transient stability of voltage-source converters with grid-forming control: A design-oriented study," *IEEE Journal of Emerging and Selected Topics in Power Electronics*, vol. 8, no. 2, pp. 1019–1033, 2020.

[5] F. V. Lopes, M. J. B. B. Davi, M. Oleskovicz, A. Hooshyar, X. Dong, and A. A. A. Neto, "Maturity analysis of protection solutions for power systems near inverter-based resources," *IEEE Trans. on Power Delivery*, vol. 39, no. 5, pp. 2630–2643, 2024.

[6] M. J. Davi, M. Oleskovicz, and F. V. Lopes, "Study on ieee 2800-2022 standard benefits for transmission line protection in the presence of inverter-based resources," *Electric Power Systems Research*, vol. 220, p. 109304, 2023.

[7] B. Kasztenny, "Distance elements for line protection applications near unconventional sources," *Schweitzer Eng. Laboratories, Inc.*, 2021.

[8] M. Bini *et al.*, "Challenges and solutions in the protection of transmission lines connecting nonconventional power sources," *48th Annual Western Protective Relay Conference*, 2021.

[9] N. Baeckeland, D. Venkatramanan, S. Dhople, and M. Kleemann, "On the distance protection of power grids dominated by grid-forming inverters," in *IEEE PES Innov. Smart Grid Tech. Conf. Europe*, 2022.

[10] D. Liu *et al.*, "Evaluation of grid-forming converter's impact on distance protection performance," in *16th International Conference on Developments in Power System Protection*, vol. 2022, 2022, pp. 285–290.

[11] C. L. Peralta, H. P. Dang, and H. N. Villegas Pico, "Searching for grid-forming technologies that do not impact protection systems: A promising technology," *IEEE Electrif. Magazine*, vol. 12, no. 2, pp. 63–70, 2024.

[12] C. L. Peralta and H. N. Villegas Pico, "Impact of grid-forming converters on distance elements based on the x and m calculations," in *2024 IEEE Texas Power and Energy Conference (TPEC)*, 2024, pp. 1–6.

[13] M. J. B. B. Davi, V. A. Lacerda, M. Oleskovicz, F. V. Lopes, and O. Gomis-Bellmunt, "Insights and challenges on the protection of grid-forming converter interconnection lines," *IEEE Journal of Emerging and Selected Topics in Industrial Electronics*, vol. 6, no. 3, pp. 1109–1118, 2025.

[14] P. Rodriguez, I. Candela, C. Citro, J. Rocabert, and A. Luna, "Control of grid-connected power converters based on a virtual admittance control loop," in *2013 15th European Conference on Power Electronics and Applications (EPE)*, 2013, pp. 1–10.

[15] G. Ziegler, *Numerical Distance Protection*, 4th ed. Publicis MCD Verlag, Feb. 2011.

[16] U. F. E. R. Commission, "Interconnection for wind energy docket no. rm05-4-001," 2005.

[17] T. Neumann, T. Wijnhoven, G. Deconinck, and I. Erlich, "Enhanced dynamic voltage control of type 4 wind turbines during unbalanced grid faults," *IEEE Trans. on Energy Conversion*, vol. 30, no. 4, pp. 1650–1659, 2015.

[18] IEEE, "Ieee standard for interconnection and interoperability of inverter based resources (ibrs) interconnecting with associated transmission electric power systems," *IEEE Std 2800-2022*, pp. 1–180, 2022.

[19] V. Lacerda, E. Prieto-Araujo, M. Chea-Mañe, and O. Bellmunt, "Phasor and emt models of grid-following and grid-forming converters for short-circuit simulations," *Electric Power Systems Research*, vol. 223, p. 109662, 10 2023.

[20] Q.-C. Zhong and G. Weiss, "Synchronverters: Inverters that mimic synchronous generators," *IEEE Trans. on Industrial Electronics*, vol. 58, no. 4, pp. 1259–1267, 04 2011.

[21] S. D'Arco and J. A. Suul, "Virtual synchronous machines-classification of implementations and analysis of equivalence to droop controllers for microgrids," in *2013 IEEE Grenoble Conference*. IEEE, 06 2013.

[22] S. D. Tavakoli, E. Prieto-Araujo, O. Gomis-Bellmunt, and S. Galceran-Arellano, "Fault ride-through control based on voltage prioritization for grid-forming converters," *IET Renewable Power Generation*, 01 2023.

[23] K. Silva and M. Almeida, "Positive sequence voltage memory filter for numerical digital relaying applications," *Electronics Letters*, vol. 51, no. 21, pp. 1697–1699, 2015.

[24] E. Schweitzer, K. Behrendt, T. Lee, and D. Tziouvaras, "Digital communications for power system protection: security, availability, and speed," in *2001 Seventh International Conference on Developments in Power System Protection (IEE)*, 2001, pp. 94–97.